Journal of
Materials Chemistry B

Materials for biology and medicine

Accepted Manuscript

This article can be cited before page numbers have been issued, to do this please use: K. Murakawa, D. R. King, T. L. Sun, H. Guo, T. Kurokawa and J. P. Gong, *J. Mater. Chem. B*, 2019, DOI: 10.1039/C9TB01376H.

ROYAL SOCIETY OF CHEMISTRY

rsc.li/materials-b

View Article Online
DOI: 10.1039/C9TB01376H

ARTICLE

Polyelectrolyte Complexation via Viscoelastic Phase Separation Results in Tough and Self-Recovering Porous Hydrogels

Kohei MURAKAWA,[a] Daniel R. KING,[bc] Taolin SUN,[bcd] Honglei GUO,[b] Takayuki KUROKAWA[bc] and Jian Ping GONG*[bce]

Received 00th January 2019,
Accepted 00th January 2019

DOI: 10.1039/x0xx00000x

Polyelectrolyte complexation between oppositely charged polyelectrolytes forms coacervates in dilute solutions and thin films in concentrated solutions. It is difficult to obtain macroscopically uniform bulk polyelectrolyte complex (PEC) materials, since the two polymers form insoluble complexes quickly at the contact interface during mixing, resulting in heterogeneous aggregates. Here, we succeeded in preparing bulk PEC materials based on desalting-induced polyelectrolyte complexation via viscoelastic phase separation. With a high ionic strength aqueous medium, a homogeneous and concentrated solution containing oppositely charged polyelectrolytes is prepared. Desalting of the counter-ions and co-ions of the solution through semi-permeable membranes induces viscoelastic phase separation of the solution to form a physical hydrogel with open pore structure. Regulating the charge ratio of the two oppositely charged polymers results in significant changes in the porous morphology and mechanical properties. The charge-balanced PEC hydrogels show unique properties including high toughness and self-recovery due to the reversible ionic associations. The porous yet tough properties of bulk PEC hydrogels makes them potential candidates for applications such as cell scaffolds.

1. Introduction

Polyelectrolyte complexation, the association process of oppositely charged polymers driven by electrostatic interactions and counter-ion release, has been widely found in specific types of soft matter.[1,2] The ionic associations formed between such macromolecules can reversibly fix and/or dissociate in specific environments (varying salt concentration, temperature, etc.), and they have important roles in many biological processes.[3] For example, DNA, which is negatively charged, is regularly folded by forming ionic associations with cationic proteins such as histone but unwinds when access to genetic information is necessary.[4–6] The fascinating properties that can be achieved through this method have led researchers to utilize polyelectrolyte complexation in synthetic applications, such as in drug delivery systems and in other biomaterials.[7–10]

Materials from polyelectrolyte complexes (PECs) exhibit unique properties. Due to the reversible associations derived from polyelectrolyte complexation, they often exhibit adhesive and self-recovery abilities.[11,12] These materials have been studied as mixtures of oppositely charged polyelectrolyte solutions, which leads to phase separation to form coacervates.[1] However, through this process, it is difficult to form macroscopically uniform structures in bulk materials, since the polymer solutions quickly form strong complexes at the contact interface and become insoluble during mixing, resulting in small aggregates.[8] Due to quick condensation, the application of PEC-based materials has been primarily limited to thin films formed at the contact interface.[13,14] Fabrication of bulk PEC materials with macroscopically uniform structures remains challenging.

In order to achieve this goal, some methods have been reported. The first method involves controlling the ionization degree in weak polyelectrolytes, where the difference in polarity between the polyelectrolytes and solvent acts as a trigger for complexation.[12] The materials formed from this process possess low charge density and are mechanically weak. Another method involves the polymerization of PEC hydrogels from monomers. In this case, to a polyelectrolyte solution, oppositely charged monomers are added and subsequently polymerized, resulting in a charge-neutral polymer hydrogel.[15] Although the hydrogels obtained by this method are tough, polymerization from monomer is technically difficult and limits the application of PEC hydrogels. Thus, new and simple strategies to develop tough PEC hydrogels with macroscopically uniform structure are required.

Here, we report a simple desalting method to produce tough, bulk PEC hydrogels. First, a homogeneous and concentrated polymer solution is prepared by dissolving oppositely charged homopolymers in a high concentration sodium chloride aqueous solution. Desalting of the counter-ions and co-ions of the solution through a semi-permeable membrane induces viscoelastic phase separation of the bulk polymer solution. The resulting PEC hydrogels show unique properties including high toughness and self-recovery after

[a] Graduate School of Life Science, Hokkaido University, Sapporo, 001-0021, Japan.
[b] Faculty of Advanced Life Science Hokkaido University, Sapporo, 001-0021, Japan
[c] Global Station for Soft Matter, Global Institution for Collaborative Research and Education (GI-CoRE), Hokkaido University, Sapporo, 001-0021, Japan
[d] South China Advanced Institute for Soft Matter Science and Technology, South China University of Technology, Guangzhou, 381st Wushan Road, Tianhe District, 510640, China
[e] Institute for Chemical Reaction Design and Discovery (WPI-ICReDD), Hokkaido University, Sapporo, 001-0021, Japan
E-mail: gong@sci.hokudai.ac.jp (J. P. Gong)

†Electronic Supplementary Information (ESI) available:
See DOI: 10.1039/x0xx00000x

View Article Online
DOI: 10.1039/C9TB01376H

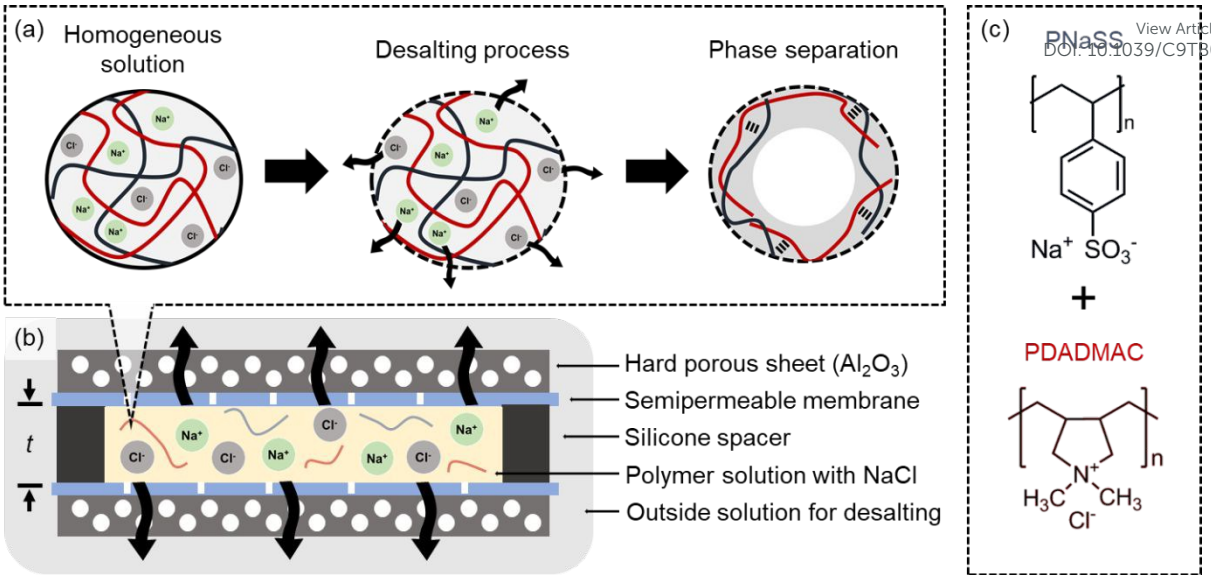

Figure 1. Schematics of preparation of the PEC hydrogels. (a) Homogeneous polyelectrolyte solution was prepared followed by the removal of counter-ions (NaCl) during the dialysis process. Absence of counter-ions promoted ionic associations between polymers, leading to phase separation of the polyelectrolyte solution, and subsequent pore formation. (b) A schematic of the mold used for desalting of the polyelectrolyte solution. The mold consisted of semi-permeable membranes supported by hard, porous alumina plates, and silicone spacers of thickness, *t*, 3 or 9 mm. (c) Chemical structure of the polymers used in this report. For strong ionic associations, polymer species with hydrophobic functional bases were selected.

deformation due to the ionic associations.[15] Interestingly, this desalting process results in the formation of inter-connected micro-scale porous structures, due to the competition between the densification that occurs during complexation of the polymer network and the enhanced viscoelasticity of the polymer (Figure 1a). Previous methods to form porous hydrogels involved techniques such as solvent casting, particle leaching, gas foaming and freeze-drying, and little is known about the porous structure induced by viscoelastic desalting.[16–19] We reveal that these micro-structures can be tuned by controlling the composition. Due to the porous structure, the mechanical response of the PEC hydrogels in compression differs from traditional non-porous hydrogels, and we hypothesize the origin of this response. Different kinds of homopolymers have also been used, demonstrating that this is a universal method to develop bulk PEC hydrogels, not dependent on specific polyelectrolyte species. The morphology of the porous structure strongly depends on the chemical species of the polymer. These bulk PEC hydrogels are expected to be used as cell scaffolds, due to their biocompatibility and structural similarity to extracellular matrices. Additionally, super-structures based on this fabrication process may have potential applications such as in separation membranes for micron-scale particles.

2. Experimental

2.1 Materials

Commercially available anionic poly (sodium 4-styrenesulfonate) (PNaSS, M_w ~200,000) solution and cationic poly (diallyldimethylammonium chloride) (PDADMAC, M_w 200,000-350,000) solution were purchased from Sigma Aldrich. Sodium chloride (NaCl) was purchased from Wako Pure Chemical Industries, Ltd., Japan. Millipore deionized water was used for all experiments.

2.2 Preparation of Polyelectrolyte Complex Hydrogels

Polyelectrolyte solutions were prepared by mixing PNaSS and PDADMAC aqueous solutions with 3.7 M NaCl at 70 ℃. The solution was poured into a mold. PEC hydrogels were formed by dialysis of the polymer solution through the semi-permeable membranes of the mold, as shown in Figure 1(b). The mold used during the desalting process consists of a semi-permeable membrane, a hard, porous alumina plate, and 3- or 9-mm silicone spacers. The semi-permeable membrane has a molecular weight cut off (MWCO) of 3,500 and the MWCO is much smaller than the M_w of polymers used in this work, preventing the polymers from passing through the membranes. The desalting process occurred in two steps. First, the mold was immersed in NaCl aqueous solutions of various concentration, C_s, for 2 days. After the initial saline immersion, the mold was immersed in deionized water for over 7 days. The samples are coded as (f-C_p-C_s), where f represents the molar fraction of the anionic monomer unit, C_p is the total monomer molar unit concentration, and C_s is the NaCl molar concentration of the outside solution used during the first step of desalting.

2.3 Characterization

2.3.1 Swelling Measurements

The swelling volume ratio, Q_v, was defined as the ratio of the sample volume at swelling equilibrium, V, to that of the solution state, V_0, $Q_v = V/V_0$. The water content of the dialyzed samples was measured by a moisture tester (MOC-120H, Shimazu Co. Japan). The water content, w_c, was defined as $w_c = (1 - m_{dry}/m_{swollen}) \times 100\%$, where $m_{swollen}$ is the weight of the samples in the swollen state and m_{dry} is in the dry state. To achieve adequate precision, three measurements were carried out on samples from different preparations.

2.3.2 Scanning Electron Microscopy

The morphology of the surfaces and cross-sections were observed by scanning electron microscopy (SEM, JSM-6010LA, JEOL Ltd.) under low vacuum pressure mode. The samples were fixed to the

substrate with carbon tape, and subsequently observed. The samples for cross-sectional observation were immersed in acetone just after the compression test to fix the structure and then dried in air. A sharp pick was used to fracture the sample. The fractured specimens were fixed to substrates with carbon tape and then observed. The average diameter and deviation of pore size was calculated from over 100 pores from each sample to achieve adequate precision.

2.3.3 Tensile Testing

Uniaxial tensile tests were carried out at 24 ℃ on a commercial tensile tester (Tensilon RTC-1150A, Orientec Co.) with samples cut into a dumbbell-shape with the dimensions of gauge length, L_0, 6 mm and width, w, 2 mm. The tensile deformation was conducted in water to prevent the hydrogels from drying, and a stretching velocity, v, of 100 mm min^{-1} was applied, giving a strain rate of $\dot{\varepsilon} = v/L_0$, 0.28 s^{-1}. The nominal stress, σ, was calculated from the load divided by the cross-sectional area of the undeformed sample. The strain, ε, was estimated from the crosshead displacement divided by L_0. The Young's modulus, E, was defined as the slope of the stress-strain curve at small strain. The work of extension, W, was calculated from the area below the stress-strain curve until fracture. To achieve adequate precision, three measurements were carried out on samples from different preparations.

2.3.4 Compression Testing

Uniaxial compression tests were carried out at 24 ℃ while submerged in water with a commercial mechanical tester (Precision Universal/Tensile Tester AG-X, Shimadzu). The samples were cut into cylinders with the following dimensions: diameter, d, of 15.2 - 15.6 mm and height, h_0, of about 6.2 mm. The samples were compressed with a compression strain, ε_c, of 0.7 with the compression strain rate, $\dot{\varepsilon}_c$, spanning from 1.7*10^{-3} to 2.1*10^{-1} s^{-1}. The nominal compression stress, σ_c, was calculated from the load divided by the circular area of the undeformed samples. The compression strain, ε_c, was estimated from the crosshead displacement divided by h_0.

2.3.5 Rheological Testing

Rheological tests were carried out while submerged in water with an ARES G2 rheometer (advanced rheometric expansion system, Rheometric Scientific Inc.). A rheological frequency sweep from 0.01 to 100 rad s^{-1} was applied with a shear strain of 0.1 % with parallel-plate geometry. The temperature was controlled from 16 - 72 ℃. The samples were cut into cylinders with the following dimensions: diameter, d, of about 16 mm and height, h_0, of about 2 mm. The samples were adhered to the plates with a cyanoacrylate-based glue (Aron alpha, TOWAGOSEI Inc.).

2.3.6 Cyclic Compression Testing

Cyclic compression was carried out at 24 ℃ while submerged in water with a commercial mechanical tester (Precision Universal/Tensile Tester AG-X, Shimadzu). The samples were cut into cylinders with the same dimensions as used in compression testing. The samples were compressed at compression strains, ε_c, of 0.03, 0.15 and 0.7, respectively. 1, 10, 100, 1,000, 5,000 and 50,000 s after the jig returned to the initial position, the samples were compressed again at the same compression strain. Each test was conducted with $\dot{\varepsilon}_c$ = 8.3*10^{-3} s^{-1}. Hysteresis area, U_{hys}, was obtained by integrating the area enclosed by one cycle of a strain-stress curve. Different samples were used for each waiting time experiment. The recovery ratio, $U_{hys\text{-}2nd}/U_{hys\text{-}1st}$*100 was calculated from the area ratio of the second hysteresis loop relative to the first.

2.3.7 Donnan Potential Measurement

To examine the electric potential of the samples and estimate the inner pore size, Donnan potential measurements were carried out with two kinds of electrodes. This measurement gives spatial Donnan potential distribution that corresponds to local charge density variation of the hydrogels. The details of this technique and how it can be used to measure the potential of hydrogels has been reported in previous studies.[20–22] Briefly, a reference electrode and a working electrode were made from a carbon electrode and glass microelectrode, respectively, as Figure S2(a) shows. The working electrode was prepared by pulling a borosilicate capillary tube (BF-100-78-15, Sutter Instrument Co.) with a micropipette puller (MODEL P-1000IVF, Sutter Instrument Co.). The pulled glass capillary, with a tip diameter of about 400 nm, was filled with 3.0 M KCl solution. A reversible silver/silver chloride electrode was inserted into the capillary. The electrode was connected to an oscilloscope (HDO6000, Teledyne LeCroy) with a high-impedance intracellular preamplifier (Model 8700 Cell Explorer, Dagan) to monitor and measure the potential difference between the two electrodes. The hydrogels were immersed in 10^{-3} M NaCl solution for over 3 days before the measurement. The insertion speed of the working electrode into the hydrogels was controlled at 197.5 nm s^{-1} by a micromanipulator (DMA-1511, Narishige). The average diameter and standard deviation of the pores was measured by the peak to peak distance of the Donnan potential depth profiles, and more than ten peaks were recorded to achieve adequate precision.

3 Result and Discussion

3.1 Bulk Composition and Swelling Behavior

Polyelectrolyte complex hydrogels (PEC hydrogels) obtain their properties and structure from the ionic associations formed between the oppositely charged polyelectrolytes. In this work, we mainly use polymer species with hydrophobic functional moieties which may induce stronger ionic associations between polymer chains as shown in Figure 1(c).[23,24] First, we examined the charge fraction, or the molar ratio of anionic to cationic species, which is a critical factor in determining the properties and structure of the resulting hydrogels.

Figure S1 shows the effect of molar fraction of the anionic monomer unit, f, on the appearance of the precursor polymer solutions at 24 °C, where the total monomer molar unit concentration, C_p, is 1.0 M in 3.7 M NaCl. The solutions appear homogeneous with increasing charge fraction until high f ($f > 0.6$), when the solution turns turbid. This apparent change in phase likely occurs because hydrophobic functional bases of PNaSS aggregate, forming clusters with an average size that is larger than the wavelength of light. This means that the presence of excess salts can shield the ionic associations between polymers at all compositions, preventing strong complexation and precipitation from occurring at the contact interface during mixing.

Compared to traditional PEC mixtures that undergo complexation at the interface, the mixtures formulated here can form bulk hydrogels by dialysis at all compositions, and these hydrogels will have macroscopically uniform structures throughout the material. Here, the composition of the PEC hydrogel is (f -1.0-0.3). The swelling behavior dramatically changes with f, as seen in Figure 2. In Figure 2(a), PEC hydrogel samples at their equilibrium swelling state in pure water are shown, and the dotted circles illustrate the size of the samples prior to dialysis of the polymer solution. These results are analyzed quantitatively in Figure 2(b), where the effect of f on the swelling volume ratio, Q_v, and water content, w_c, of the PEC samples is plotted. The measurements were carried out over a wide composition range (f = 0.3 – 0.7) and uniform hydrogels were obtained for all compositions. Around the charge balanced composition (f = 0.49 – 0.53), the samples decreased in volume during dialysis compared to the solution state (Q_v < 1). On the other hand, with compositions consisting of significant charge imbalance (f < 0.49; f > 0.53), the samples swelled (Q_v > 1). This indicates that around the charge balance point, the complexation process reaches maximum conversion, resulting in strong bonding. However, when the charge composition is unbalanced, some charged bases cannot form ionic associations and the dissociated small molecule counter-ions cause an osmotic pressure gradient, resulting in significant swelling.[25]

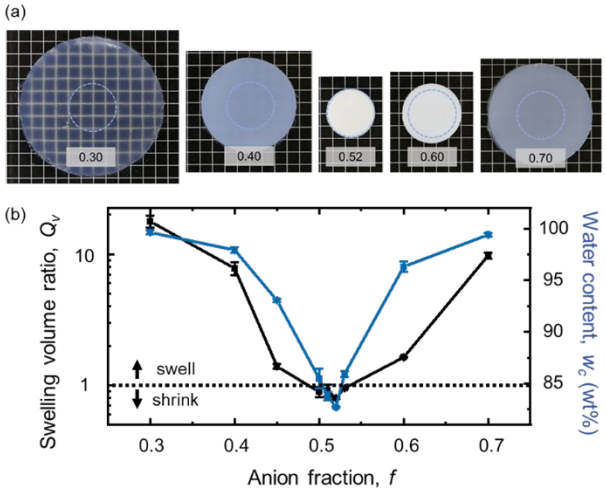

Figure 2. Appearance and swelling behavior of PEC hydrogels (f-1.0-0.3) prepared with different anion fraction, f = 0.3 – 0.7. (a) Appearance of PEC hydrogels at the equilibrium state in water prepared with different anion fraction, f, ranging from 0.3 to 0.7. The dashed circles represent the size of the polymer solution before dialysis. (b) The swelling volume ratio, Q_v, and water content, w, versus the anion fraction, f.

3.2 Morphology

When the hydrogels are compressed, water is easily squeezed out of the samples, and after the force is removed, the water can be quickly re-absorbed, as shown in Figure 3(a) and Video S1. This characteristic indicates that hydrogels possess an inter-connected porous structure.[26] For the samples fabricated here, the desalting process that occurs during dialysis of the polyelectrolyte mixture causes inter-connected porous structures to develop. This mechanism represents a novel method to create porous hydrogels compared to previous methods like solvent casting, particle leaching, gas foaming, and freeze-drying. In the dialysis process, the polymer chains cannot move freely because of entanglement, while the bonds formed due to ion complexation result in solidification and gelation of the structure as shown in Figure 1(a). Understanding the process of phase separation in these systems is key towards understanding the morphology of the resulting porous hydrogels.

Figure 3(b) shows SEM images of the surface of the PEC hydrogels with f content ranging from 0.3 to 0.7. Porous structures are observed for all surfaces. The diameter of the surface pores was determined from SEM images and the results of the measurements can be seen in Figure 3(c). The hydrogels formulated near the charge balance composition (f = 0.52) have pores that range in size from 10 to 30 μm on the surface. There are large differences between the porous surface structures of the positively and negatively charged hydrogels, even though their volume changes are almost the same. The negatively charged samples (f = 0.6, 0.7) have pores of 40 and 60 μm on average with standard deviations of 16 and 34 μm, respectively, and have thick polymer walls. On the other hand, it is difficult to define the pore size in the positively charged hydrogels (f = 0.4, 0.3) because of their comparatively thin polymer walls. The difference in pore morphology is due to polymer structure of the majority component, rather than the overall swelling ratio of the hydrogel. The anionic polymer, PNaSS, repeat unit contains a benzene ring, which tend to aggregate due to π- π interactions. Therefore, the negatively charged hydrogels that have higher concentrations of PNaSS would form thick polymer walls compared to charge-neutral or positively charged hydrogels. When the majority component is changed to an anionic polymer without benzene rings, such as poly (2-acrylamido-2-methylpropane sulfonic acid) (PNaAMPS), there is no large difference in the pore structure between the negatively and positively charged hydrogels (f = 0.7 and 0.3, respectively) (Figure S3).

While we can easily examine the surface morphology by SEM observation, quantifying the internal morphology is more difficult. Fracturing or cutting the sample will disrupt the internal structure, preventing their use to analyze the internal structure. We therefore utilize a new method to infer the internal structure, by measuring the Donnan potential as a function of depth as seen in Figure S2. This experiment measures the electric potential at specific locations within the PEC hydrogels. We expect that the electric potential within the polymer walls (high charge density) and the pores (neutral solvent) to vary greatly, and by measuring the local potential as a function of depth we can quantify the internal pore structure. The pore size in the hydrogels in the wet state is estimated from the distances between each peak in the absolute value of electrical potential as Figure S2(b) and (c) show. The sizes of the inner pores estimated from the Donnan potential measurements are also shown in Figure 3(c). The results are consistent with the sizes recorded from the SEM micrographs of the surface. This means the inner pore structure is likely similar with the structure observed on the surface. The large standard deviation of the Donnan potential in Figure 3(c) is mainly due to the microelectrode insertion location. The microelectrode does not always penetrate through the center of the pores, and the closer to the edge that insertion occurs, the smaller the apparent pore size becomes. Interestingly, the potential between peaks does not return to 0 mV as Figure S2(b)

View Article Online
DOI: 10.1039/C9TB01776H

shows. This indicates some charged species remain in the porous structure even after more than one week of dialysis.

1.2, and the surfaces of samples with high polymer concentration (C_p ≧ 1.4 M) do not have pores on the surface, while they have a porous

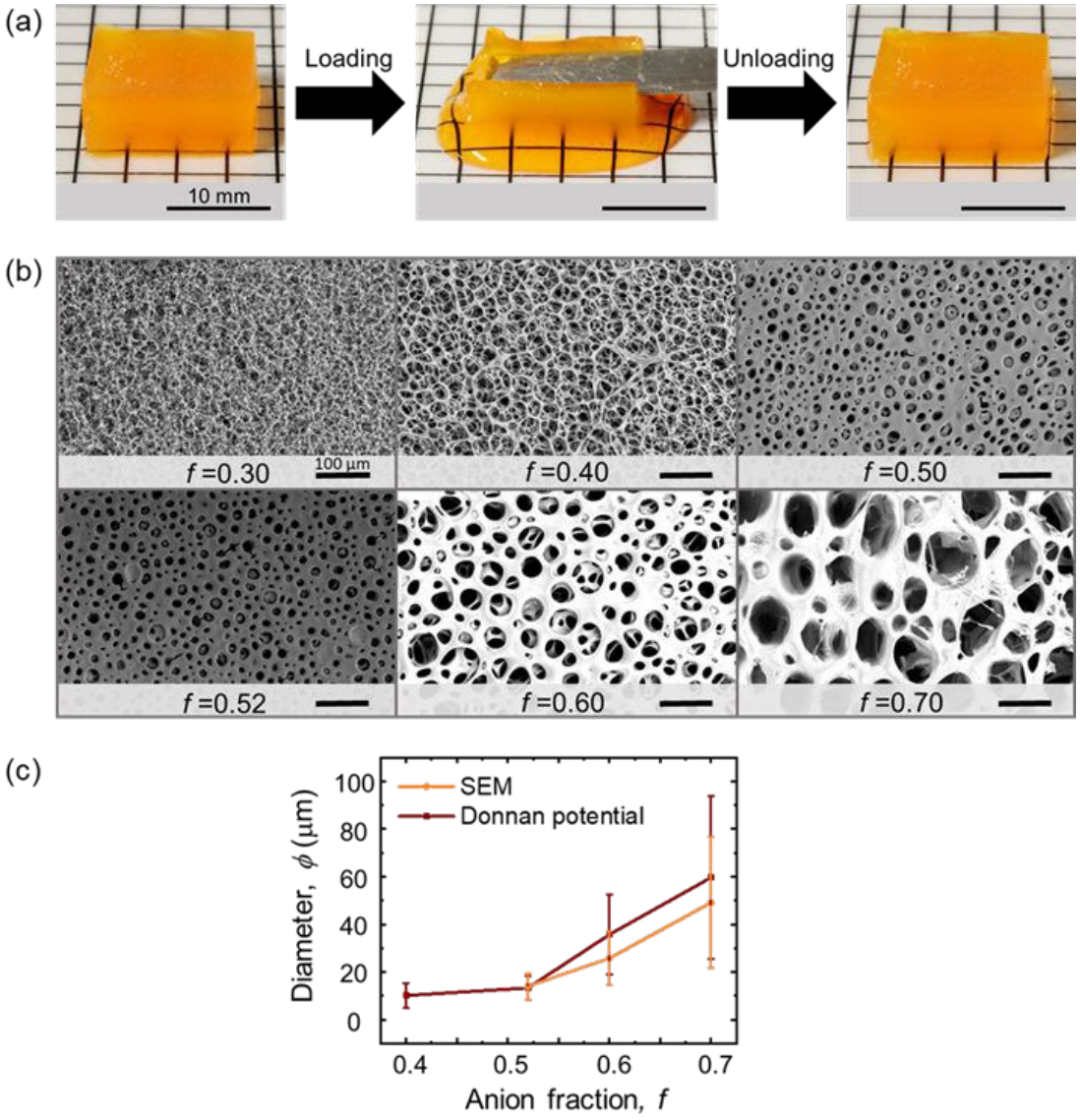

Figure 3. Morphology of PEC hydrogels (*f*-1.0-0.3) prepared with different anion fraction, *f = 0.3 – 0.7*. (a) Appearance of a compressed PEC hydrogel with *f* = 0.7. Some water easily goes out from the hydrogels during compression. After removal of the compression force, the water is quickly absorbed by the sample. This drainage behavior can be repeated. The sample and water were dyed with methyl orange for clarity. All the samples show drainage by compression, regardless of anion fraction. (b) SEM micrographs of the surfaces of the PEC samples prepared with different anion fraction, *f*. The micrographs were taken in the wet state under a low vacuum pressure mode. (c) The diameter, ϕ, of the surface pores determined from SEM images of the sample surface, and of inner pores within the bulk, estimated from Donnan potential measurements.

We also examine the effect of the other parameters (C_p and C_s) on the swelling behavior and morphology for charge balanced composition (f = 0.52). The results on the effect of these parameters (C_p and C_s) are shown in Figure S4 and Figure S5, respectively. Polymer concentration, C_p, is one of the critical factors in determining the properties of the PEC hydrogels. Uniform, and bulk hydrogels can be formed with sufficiently high C_p (C_p ≧ 0.8 M). The hydrogels shrink (Q_v < 1) with C_p ≦ 1.0 M, and swell (Q_v > 1) with C_p ≧ 1.2 M as seen in Figure S4(b). Interestingly, even when the charge is balanced, the samples swell with high polymer concentration. Figure S4(c) shows SEM images of the surfaces. The porous structure that forms at C_p = 0.8 is different from the structure formed at C_p = 1.0 and interior. The surface without porous structure might work as a semipermeable membrane, where counter-ions and co-ions cannot easily diffuse out in comparison to water molecules that can diffuse in, which causes the swelling behavior described above.[27]

Salt concentration in the solution used for the first dialysis step, C_s, also affects the properties of the PEC hydrogels because it influences the relaxation time of ionic bonds. The dialysis environment with high salt concentration allows the ionic associations to relax and with low salt concentration fixes the complexes quickly. Figure S5(a) presents the effect of C_s on the swelling volume ratio, Q_v, and water content, w_c, and Figure S5(b) contains SEM images of the surfaces. The hydrogels shrink more with high salt concentration,

although a large difference cannot be observed on the surface. This might be because the high salt concentration dialysis environment causes the desalting process to occur more slowly and relaxes the ionic associations to a more stable state, without a porous structure. From these results, we see that the porous structure on the surface can be affected by polymer concentration and salt concentration in the solution used for the first dialysis step, but the mechanism is not straightforward.

3.3 Mechanical Properties

It is known that hydrogels fabricated from polyelectrolyte complexes achieve maximum toughness at the charge balance point.[25] When charged pairs form, they can reversibly dissociate and associate during deformation to release stress. These weak bonds contribute significant hysteresis to the system, resulting in mechanically tough hydrogels. To maximize the mechanical properties of the porous hydrogels, we modified the charge fraction of the hydrogels and measured the mechanical response in tension. The difference in ionic associations with respect to charge ratio largely influences the mechanical properties as seen in Figure 4(a) and Figure 4(b). Figure 4(a) shows the stress – strain curves from tensile tests of each samples and Figure 4(b) shows the modulus and work of extension calculated from the curves. The hydrogels near the charge balance composition ($0.49 < f < 0.53$) have excellent properties. The toughest samples are obtained with a charge fraction of 0.51 and 0.52, with a modulus of over 7.0 MPa and a strain energy density of over 2.75 MJ/m^3. We hypothesize two reasons why the charge balance point occurs not at $f = 0.5$ but between $f = 0.51$ and 0.52. One reason is because of filtration of low molecular weight polymer during dialysis. If some leakage of anionic polymer occurs during the dialysis process, this can be compensated for by a slight increase in the anionic charge fraction during polymerization. Another reason is depending on the chemistry of the functional groups, the effective charge of the polyelectrolytes may slightly differ. The presence of the phenyl rings near the sulfonate group in the PNaSS polymer may influence the local electron density, resulting in a slight variance in valency. Increasing the charge fraction allows us to overcome this natural imbalance.

From these results, we defined the charge balance point as the point when the hydrogels exhibit optimized mechanical properties. We can quantitatively prove that the charge balance point occurs at this charge ratio by measuring the Donnan potential. When the Donnan potential registers as 0 mV, charge balance has been achieved. The Donnan potential shifts from positive to negative between $f = 0.51$ and 0.52, which means the compositions that are the closest to neutral are between $f = 0.51$ and 0.52 as Figure S2(c) shows. This is consistent with the tensile test results shown in Figure 4(b). This Donnan potential technique is a quick, precise method to measure the charge balance point to optimize the mechanical response of PEC hydrogels.

The mechanical properties decrease as the hydrogel becomes charge imbalanced ($f < 0.49$, $f > 0.53$). In the charge imbalanced state, two events occur: the samples swell significantly, decreasing the polymer density, and a lower concentration of complexation sites exist, resulting in less sacrificial bonds and therefore decreased energy dissipation during deformation.[28] Both of these events cause the mechanical strength and toughness of the hydrogels to decrease.

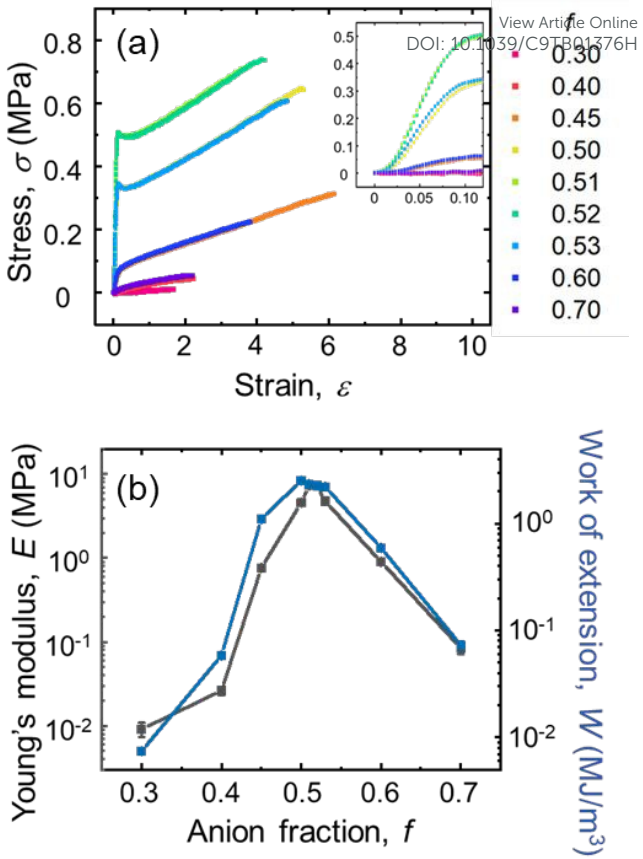

Figure 4. Tensile behaviors of PEC hydrogels (*f*-1.0-0.3) prepared with different anion fraction, $f = 0.3 – 0.7$. (a) Tensile stress – strain curves (strain rate: 0.28 s^{-1}) of the PEC samples of different anion fraction, *f*. (b) Young's modulus and work of extension of the PEC samples of different anion fraction, *f*.

3.4 Influence of Strain Rate on Compressive Response

The fabricated porous hydrogels are similar to extracellular matrices in structure and water content. To apply these materials to engineering fields, understanding the compression behavior is crucial, because the mechanical response of porous materials varies significantly from most solid materials. During compression of a typical porous material, linear elastic deformation occurs at small strain, followed by a strain softening plateau region, due to either yielding or bending deformation of the porous structure. As compression continues, the structure becomes increasingly dense. Finally at high strain, the lack of pores and the high density results in significant strain hardening.[29,30] Here we will analyze the mechanical response of a porous hydrogel, where the pore structure contains free water.

Compression tests were performed on samples with the toughest formulation with a composition of (0.52-1.0-0.3). Figure 5(a) contains the stress – strain curves from the compression tests with different compression rates. During the linear elastic small strain region, as strain rate increases, the slope increases, representing an increase in modulus. At intermediate strain, stress varies little with strain, but the highest strain rate sample experiences the highest plateau stress. At a high strain of 0.7, the stress increases from 1.5 to 3.5 MPa with increasing compression strain rate and the hydrogel pore structure exhibits a different morphology after compression (Figure 5(b)). The pore structure yields at low strain rate and bends at high strain rate,

implying that deformation is strain rate dependent. These dynamic behaviors could be attributed to two factors: the influence of strain rate on viscoelasticity, and the drainage of incompressible water from the sample.

5(a). In the low strain region, the high strain rate sample exhibits higher stiffness.

View Article Online
DOI: 10.1039/C9TB01376H

In the intermediate strain region, deformation becomes more complicated. Viscoelastic effects due to strain rate still play a role,

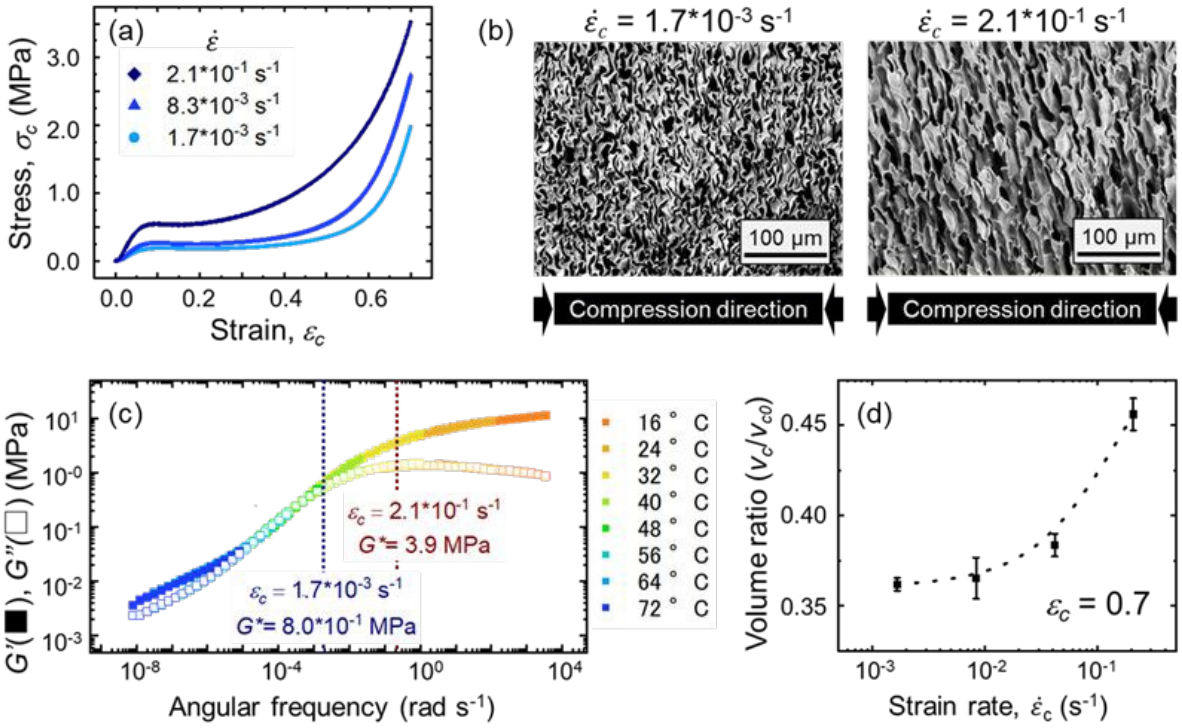

Figure 5. Strain rate dependence of PEC hydrogels (0.52-1.0-0.3) while undergoing compression and dynamic mechanical properties. (a) Stress-strain curves of the PEC hydrogels with different compression strain rates. (b) SEM micrographs of the cross-sections of the compressed samples with different compression rates. The micrographs were taken under a low vacuum pressure mode. (c) Angular frequency dependence of the storage modulus, *G'*, (filled symbol) and loss modulus, *G''*, (open symbol). The rheological test was carried out with a frequency sweep spanning from 0.01 to 100 rad s^{-1} with a shear strain of 0.1 % in parallel-plate geometry. The temperature was controlled from 16 to 72 ℃. The master curves were obtained by performing classical time-temperature superposition shifts with a reference temperature of 24 ℃. The dotted lines represent angular frequencies that correspond to compression strain rates of, $1.7*10^{-3}$ and $2.1*10^{-1}$ s^{-1}. (d) The volume ratio, v_c/v_{c0}, as a function of strain rate, $\dot{\varepsilon}_c$. v_c is the volume after compression and v_{c0} is the volume before compression. The dash curve is drawn as a guide for the eyes. The samples were cut into cylinders with the following dimensions: diameter, *d*, of 15.2 - 15.6 mm and height, h_0, of about 6.2 mm.

Hydrogels that possess dynamic bonds exhibit strong viscoelasticity. In the case of PEC hydrogels, dynamic bonds are contributed by ionic associations. At higher strain rate, more ionic associations exist on the observation time-scale, resulting in high modulus. As the strain rate decreases, ionic associations can relax prior to fracture, resulting in a softer hydrogel. These characteristics can be seen in Figure 5(c), from the results of shear rheology performed on the PEC hydrogel. Small strain was applied so that pore structure deformation can be neglected. Classical time temperature superposition was performed at a reference temperature of 24°C. The shift factors, a_T, are listed in Figure S6. The complex modulus, G^*, (= $(G'^2+G''^2)^{1/2}$) at an angular frequency corresponding to a compression strain rate of $2.1*10^{-1}$ s^{-1} in the rheological measurements is about 5 times higher than the complex modulus at an angular frequency corresponding to a compression strain rate of $1.7*10^{-3}$ s^{-1}. Furthermore, at higher frequency, the tan δ (= G''/G') is lower, demonstrating that at high frequencies the gels possess more solid-like character. These results agree with the tests performed in Figure

specifically influencing the morphology of the pores due to different deformation mechanisms. However, the rate at which water contained within the pore structure is capable of escaping will also influence the mechanical response. Due to the viscoelastic character of the gel, at low strain rates the polymer walls are soft and can yield easily due to ionic bond relaxation, as tan δ is large. Furthermore, a sufficiently long time is required for the water to escape, which along with the soft polymer response allows for water drainage to occur with minimal stress. At high strain rates, the pore walls exhibit increased modulus and low tan δ, and they bend rather than yield. Due to the incompressibility of water, and the relatively stiff pore structure, stress increases as water is forced out of the structure. The results of these effects can be seen by comparing the pore structures of low and high strain rates samples (Figure 5(b)). This hybrid deformation mechanism causes the higher strain rate tests in Figure 5(a) to exhibit higher stress during the intermediate strain regime. The combination of hydrogel viscoelasticity and water drainage rate work together to cause the unique mechanical properties seen in porous hydrogels.

View Article Online
DOI: 10.1039/C9TB01376H

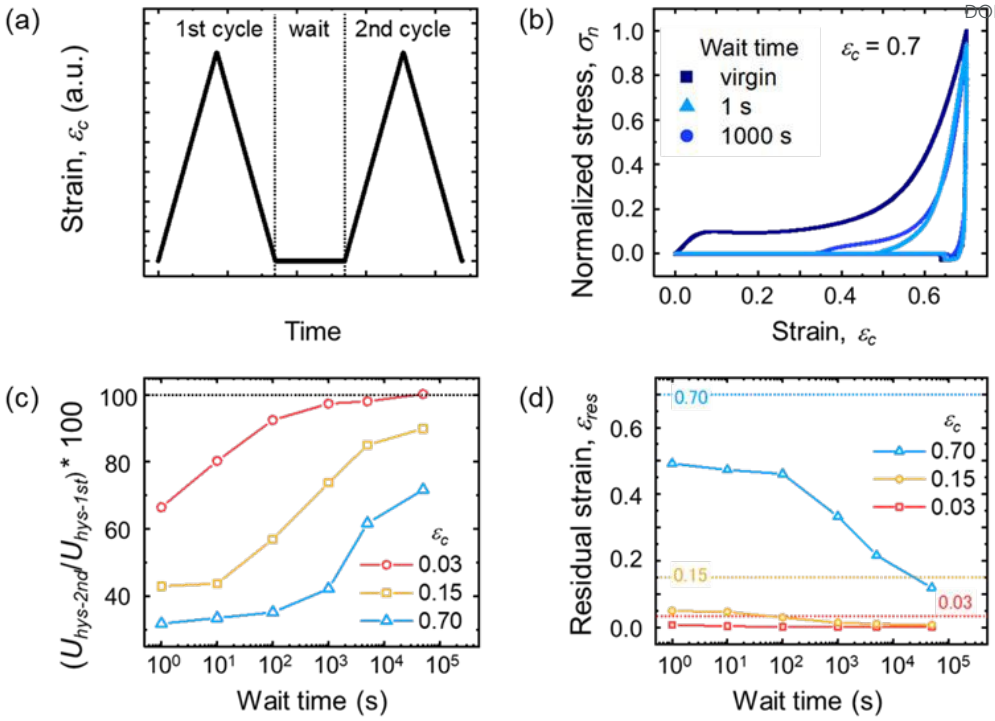

Figure 6. Self-recovery ability on the compression behavior of PEC hydrogels (0.52-1.0-0.3). (a) An exemplary schematic of applied compressive strain, ε_c versus time for the self-recovering experiment. (b) Normalized stress-strain curves from cyclic compression tests at ε_c = 0.7 with $\dot{\varepsilon}_c$ = 8.3*10^{-3} s^{-1}. The figure only shows the cyclic curves for waiting times of 1 and 1,000 s. Normalized stress, σ_n, is calculated from the compression stress divided by the compression stress of the first cycle at ε_c = 0.7. (c) Waiting time dependence of the recovery in hysteresis (ratio of the hysteresis energy of the second loop to the first loop). The dotted line represents 100 % recovery of hysteresis. (d) Waiting time dependence of the recovery in residual strain, ε_{red}. The blue, yellow and red dotted lines represent compression strains 0.7, 0.15 and 0.03, respectively. Different samples were used for each waiting time experiment.

The strain rate dependence in the high strain region is primarily governed by the mechanical properties of the densified PEC hydrogel. Similar to the low strain region, PEC hydrogel viscoelasticity (increasing strain rate results in higher modulus) will influence the stiffness during compression. However, depending on the deformation mechanisms of the intermediate strain region, the volumes of the samples will differ (Figure 5(d)). The samples compressed at higher strain rate have a larger diameter, and therefore possess larger volumes of trapped water. Water is incompressible and has high bulk modulus (~2 GPa), increasing the force required to deform the sample. Therefore, the combination of high modulus at high strain rate and the presence of trapped water causes the high strain rate sample to exhibit high stress at large compression.

3.5 Self-Recovery After Compressive Deformation

The ionic associations of PEC hydrogels are capable of reforming after dissociation. We investigated the porous hydrogels self-recovery ability by conducting cycle tests on the toughest sample (0.52-1.0-0.3) at different compression strains (strain = 0.03, 0.15, 0.7). These three strains were specifically chosen, as they correspond to the linear elastic region, plateau region, and strain hardening region, respectively. Cyclic compression strain, ε_c, is applied to the sample as show in Figure 6(a) with different waiting times. Figure 6(b) shows the normalized stress-strain curve from the cyclic compression test at ε_c = 0.7 with $\dot{\varepsilon}_c$ = 8.3*10^{-3} s^{-1}. The normalized stress-strain curves at other strains are reported in Figure S7. With increasing waiting time, the hysteresis of the second cycle increases. As Figure 6(c) shows, the hydrogels exhibit self-recovery abilities at all strains. At a strain of 0.03, the hydrogels fully recover 5.0*10^4 seconds after the first compression. Even after 70 % compression, the samples show over 75 % recovery 5.0*10^4 seconds after the first compression. This recovery comes from the dynamics of the physical bonds and re-absorbed water. The relatively weak bonds are easy to break during loading, and the broken pairs can then reform with nearby pairs, recovering the toughness. Re-absorbed water also can contribute to recovering the toughness due to the stress required to drain the water.

Recovery occurs not only in hysteresis but also in the thickness, as Figure 6(d) shows. At all strains, the thickness recovery trends with hysteresis recovery. The recovery of the porous structure is also observed, as seen in Figure S8. The recovery in structure along with strong hysteresis indicates that the hydrogels possess both weak ionic associations and a long polymer chain reptation time, since no covalent crosslinking is used in these formulations. The polymer chains have no relative motion by compression during the observed time-scale and maintain the global state of the structure. This is consistent with the result that the PEC hydrogels have low apparent activation energy (~ 191.1 kJ mol^{-1}) and higher apparent activation energy (~382.3 kJ mol^{-1}) than covalent bond dissociation energy (~347 kJ mol^{-1}) as Figure S6 shows. The apparent activation energy value, E_a, was estimated from the slope of the line using the Arrhenius equation $a_T = Ae^{Ea/RT}$, where a_T is the shift factor, R is the ideal gas constant, and A is a constant value, and the shift factors come from

time-temperature superposition at a reference temperature of 24 °C.[25,31] This high apparent activation energy between polymers makes the PEC hydrogels tough even without any covalent crosslinking.

4 Conclusion

In summary, we demonstrated a new, simple method to develop bulk PEC hydrogels with macroscopically uniform structure. The PEC hydrogels were formed by dialysis of a homogeneous polyelectrolyte solution containing concentrated polyanions and polycations. The materials have an inter-connected micro-scale porous structure derived from viscoelastic phase separation via desalting. The properties and morphology can be tuned by modifying the formulation of the hydrogel, such as the molar fraction of the anionic monomer unit. Concerning the mechanical properties, the charge balanced samples show the highest modulus of over 7.0 MPa and a strain energy density of over 2.75 MJ/m^3 during tensile tests, even though they are porous and contain high concentrations of water. Due to the ionic associations and porous structure, the materials show strong strain rate dependence during compression, due to the rupture mechanism of weak bonds in the PEC, as well as the influence of water draining from the porous bulk material. Ionic associations and porous structure also give rise to the hydrogel self-healing abilities. Such tough porous hydrogels are good candidates for not only cell scaffolds but also new potential applications such as separation membranes for micron-scale particles.

Conflicts of interest

There are no conflicts to declare.

Acknowledgements

This research was supported by JSPS KAKENHI Grant Numbers JP17H06144, and JP17H06376. Institute for Chemical Reaction Design and Discovery (ICReDD) was established by World Premier International Research Initiative (WPI), MEXT, Japan.

References

1 Raymond M. Fuoss and Hussein Sadek, *Science*, 1949, **110**, 552–554.
2 A. S. Michaels, *Ind. Eng. Chem.*, 1965, **57**, 32–40.
3 S. F. Banani, H. O. Lee, A. A. Hyman and M. K. Rosen, *Nat. Rev. Mol. Cell Biol.*, 2017, **18**, 285–298.
4 S. Chong, C. Dugast-Darzacq, Z. Liu, P. Dong, G. M. Dailey, C. Cattoglio, A. Heckert, S. Banala, L. Lavis, X. Darzacq and R. Tjian, *Science*, 2018, 361, eaar2555
5 D. Hnisz, K. Shrinivas, R. A. Young, A. K. Chakraborty and P. A. Sharp, *Cell*, 2017, **169**, 13–23.
6 V. A. Bloomfield, *Curr. Opin. Struct. Biol.*, 1996, **6**, 334–341.
7 J. M. Ting, H. Wu, A. Herzog-Arbeitman, S. Srivastava and M. V. Tirrell, *ACS Macro Lett.*, 2018, **7**, 726–733.
8 J. van der Gucht, E. Spruijt, M. Lemmers and M. A. Cohen Stuart, *J. Colloid Interface Sci.*, 2011, **361**, 407–422.
9 S. Farris, K. M. Schaich, L. S. Liu, L. Piergiovanni and K. L. Yam, *Trends Food Sci. Technol.*, 2009, **20**, 316–332.
10 M. George and T. E. Abraham, *J. Control. Release*, 2006, **114**, 1–14.
11 R. J. Stewart, C. S. Wang and H. Shao, *Adv. Colloid Interface Sci.*, 2011, **167**, 85–93.
12 Q. Zhao, D. W. Lee, B. K. Ahn, S. Seo, Y. Kaufman, J. N. Israelachvili and J. H. Waite, *Nat. Mater.*, 2016, **15**, 407–412.
13 G. Decher, *Science*, 1997, **277**, 1232–1237.
14 H. Ai, S. A. Jones and Y. M. Lvov, *Cell Biochem. Biophys.*, 2003, **39**, 23–43.
15 F. Luo, T. L. Sun, T. Nakajima, T. Kurokawa, Y. Zhao, K. Sato, A. Bin Ihsan, X. Li, H. Guo and J. P. Gong, *Adv. Mater.*, 2015, **27**, 2722–2727.
16 N. Annabi, J. W. Nichol, X. Zhong, C. Ji, S. Koshy, A. Khademhosseini and F. Dehghani, *Tissue Eng. Part B Rev.*, 2010, **16**, 371–383.
17 L. Draghi, S. Resta, M. G. Pirozzolo and M. C. Tanzi, *J. Mater. Sci. Mater. Med.*, 2005, **16**, 1093–1097.
18 R. Ricciardi, G. D'Errico, F. Auriemma, G. Ducouret, A. M. Tedeschi, C. De Rosa, F. Lauprêtre and F. Lafuma, *Macromolecules*, 2005, **38**, 6629–6639.
19 P. A. M. Lips, I. W. Velthoen, P. J. Dijkstra, M. Wessling and J. Feijen, *Polymer*, 2005, **46**, 9396–9403.
20 H. Guo, T. Kurokawa, M. Takahata, W. Hong, Y. Katsuyama, F. Luo, J. Ahmed, T. Nakajima, T. Nonoyama and J. P. Gong, *Macromolecules*, 2016, **49**, 3100–3108.
21 T. F. Shklyar, a. P. Safronov, O. a. Toropova, G. H. Pollack and F. a. Blyakhman, *Biophysics*, 2011, **55**, 931–936.
22 F. A. Blyakhman, A. P. Safronov, A. Y. Zubarev, T. F. Shklyar, O. A. Dinislamova and M. T. Lopez-Lopez, *Sensors Actuators A Phys.*, 2016, **248**, 54–61.
23 J. Fu, H. M. Fares and J. B. Schlenof, *Macromolecules*, 2017, **50**, 1066–1074.
24 R. Shi, T. L. Sun, F. Luo, T. Nakajima, T. Kurokawa, Y. Z. Bin, M. Rubinstein and J. P. Gong, *Macromolecules*, 2018, **51**, 8887–8898.
25 F. Luo, T. L. Sun, T. Nakajima, D. R. King, T. Kurokawa, Y. Zhao, A. Bin Ihsan, X. Li, H. Guo and J. P. Gong, *Macromolecules*, 2016, **49**, 2750–2760.
26 T. Sedlačík, V. Proks, M. Šlouf, M. Dušková-Smrčková, H. Studenovská and F. Rypáček, *Biomacromolecules*, 2015, **16**, 3455–3465.
27 H. Guo, T. Nakajima, D. Hourdet, A. Marcellan and C. Creton, 2019, **1900702**, 1–8.
28 T. L. Sun, T. Kurokawa, S. Kuroda, A. Bin Ihsan, T. Akasaki, K. Sato, M. A. Haque, T. Nakajima and J. P. Gong, *Nat. Mater.*, 2013, **12**, 932–937.
29 F. A. Blyakhman, A. P. Safronov, A. Y. Zubarev, T. F. Shklyar, O. G. Makeyev, E. B. Makarova, V. V Melekhin, A. Larrañaga and G. V Kurlyandskaya, *Results Phys.*, 2017, **7**, 3624–3633.
30 J. Zhang, L. Wu, D. Jing and J. Ding, *Polymer*, 2005, **46**, 4979–4985.
31 K. J. Henderson and K. R. Shull, *Macromolecules*, 2012, **45**, 1631–1635.

View Article Online
DOI: 10.1039/C9TB01376H

View Article Online
DOI: 10.1039/C9TB01376H

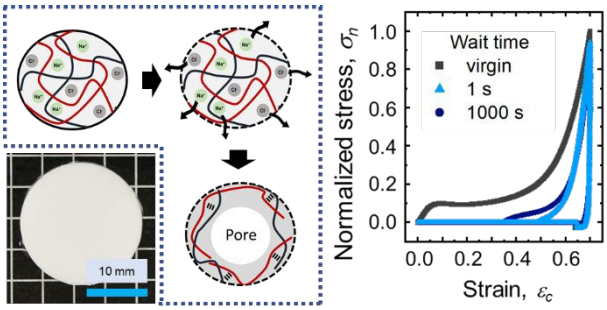

Polyelectrolyte complexation is utilized to create bulk, porous hydrogels with high toughness and self-recovery due to reversible ionic associations